Towards Unified Keyframe Propagation Models

Patrick Esser[1]   Peter Michael[1,2]   Soumyadip Sengupta[2]

[1]Runway ML   [2]University of Washington
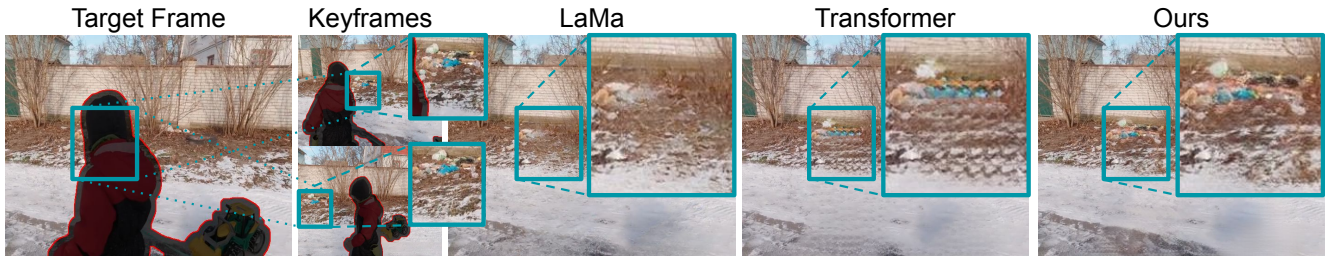
https://github.com/runwayml/guided-inpainting

Figure 1. Single image inpainting approaches such as LaMa [27] (third col.) cannot propagate context from keyframes (second col.) to a target frame (first col.). By aggregating features globally across frames, transformer-based approaches (fourth col.) can propagate coarse context about a blue object that is visible in the keyframes but not in the target frame. However, it fails to propagate high-frequency details about object locations and textures, resulting in repetitive patterns and artifacts. By modeling both local and global interactions within and across frames, our approach (last col.) successfully propagates high-frequency context and accurately reconstructs the background.

Abstract

Many video editing tasks such as rotoscoping or object removal require the propagation of context across frames. While transformers and other attention-based approaches that aggregate features globally have demonstrated great success at propagating object masks from keyframes to the whole video, they struggle to propagate high-frequency details such as textures faithfully. We hypothesize that this is due to an inherent bias of global attention towards low-frequency features. To overcome this limitation, we present a two-stream approach, where high-frequency features interact locally and low-frequency features interact globally. The global interaction stream remains robust in difficult situations such as large camera motions, where explicit alignment fails. The local interaction stream propagates high-frequency details through deformable feature aggregation and, informed by the global interaction stream, learns to detect and correct errors of the deformation field. We evaluate our two-stream approach for inpainting tasks, where experiments show that it improves both the propagation of features within a single frame as required for image inpainting, as well as their propagation from keyframes to target frames. Applied to video inpainting, our approach leads to 44% and 26% improvements in FID and LPIPS scores.

1. Introduction

To satisfy the ever-increasing demand for video content, new solutions for fast and simple video creation are required. By reducing the need for tedious frame-by-frame operations, machine learning can help creators to focus on the creative aspects of story-telling. A promising approach to reduce manual work without limiting creativity is based on keyframe propagation, where the desired result is specified on a few frames and automatically propagated to the entire video. This formulation and the need to propagate context across frames is common to many video editing tasks. For example, to separate foreground objects from the background, object selection masks must be propagated, to stylize videos, artistic edits of frames must be propagated, and to remove objects from videos, the background must be propagated from frames where it is visible (see Fig. 1).

Given this commonality, it is natural to ask whether a single unified approach can handle all of these tasks. A promising candidate for such a solution is a transformer [30] based architecture. Not only has it been a driving force of consolidation across a wide range of tasks and modalities [10,11], but, by relying on global, affinity-weighted feature aggregation, it has the potential to propagate context between multiple non-aligned frames. Furthermore, transformers and related approaches that globally aggregate features have been successfully applied to object mask propagation [4, 22].
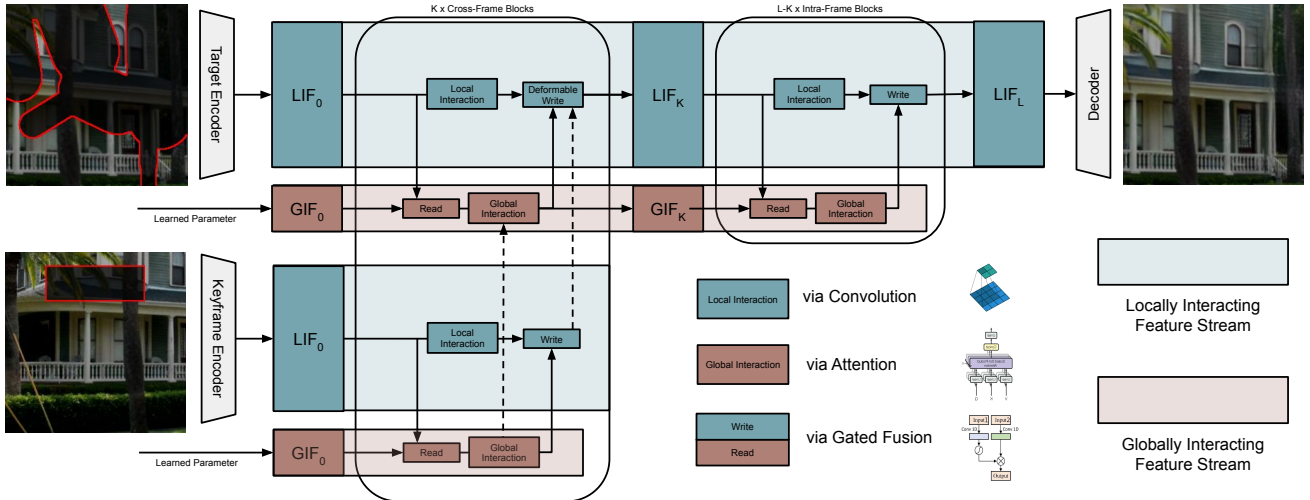
1

Figure 2. Overview of our model operating with two streams: A locally interacting feature (LIF) stream, relying on convolutions for high-frequency modeling, and a globally interacting feature (GIF) stream, relying on attention for low-frequency modeling.

However, Fig. 1 shows that a direct adaptation of transformers to keyframe-guided inpainting for object removal fails to propagate details about the background from keyframes. This observation is in agreement with the findings of [24], that global feature aggregation via attention acts as a low-pass filter, which hinders propagation of high-frequency details. Based on this, we present a two-stream model consisting of a stream of locally interacting features (LIF) and a stream of globally interacting features (GIF). To avoid loss of high-frequency details, LIF operates on a high-resolution representation and uses local convolutional operations, which exhibit the opposite behavior of attention and act as high-pass-filters [24]. High-frequency details are then propagated with a deformable feature aggregation between LIF streams of different frames, whereas robust low-frequency features are propagated with attention in the GIF stream. (see Fig. 2). Experiments demonstrate that this design improves propagation both within a single frame, evaluated via image inpainting, as well as across frames, evaluated via guided image inpainting and video inpainting.

2. Background

Transformers in Vision Following the success of transformers in natural language processing [26, 30], their architecture has been widely adopted for vision tasks [6, 12]. While the attention mechanism is permutation invariant and can model all pairwise feature interactions, its quadratic complexity with respect to input length requires adaptions for high-dimensional image data [10]. Many vision-specific modifications such as windowed attention [17] introduce assumptions about possible interactions and thus require aligned input data, making them unsuitable for keyframe propagation. Other adaptations are based on approximative attentions mechanisms [5, 31] or attention on compressed representations [7, 20] which introduces a bottleneck for propagating features. Even without such bottlenecks, recent work [24] shows that the attention mechanism is inherently biased towards low-frequency features. Hence, we aim to better understand what is required for faithful propagation of both low- and high-frequency content in order to get closer to a unified approach for keyframe propagation.

Frame Propagation Propagation of information such as color or object masks across video frames can be formulated as optimization problems [1, 15]. Since these lead to slow runtimes, deep learning-based approaches have been explored as faster alternatives [19, 37] or as more accurate but slower alternatives [3] by fine-tuning models per video. Instead of relying on a sequential forward propagation through the video, space-time memory networks [22], which bear resemblance to single-layer transformers, enable propagation of object masks from arbitrary keyframes.

Inpainting Patch-based synthesis [2, 32] provides an elegant framework that demonstrates how both image- and video-inpainting can be formulated as propagation problems. For improved runtimes and to benefit from learned data priors, deep learning-based solutions have been proposed for image [18, 21, 27, 34, 36, 38] and video inpainting [8, 9, 13, 14, 23, 33, 35]. Most video inpainting approaches rely on sequential forward prediction in time, which limits their applicability in interactive scenarios. Closest to our work on keyframe-guided inpainting are [41] and [39], but both rely on accurate estimation of scene geometry for alignment between frames, which limits applications to static scenes [39]. In contrast, we only utilize a very rough alignment based on optical flow which is interpolated in masked areas. While this introduces errors and deformations, our model can detect and correct them based on local and global feature interactions (see Fig. 3).
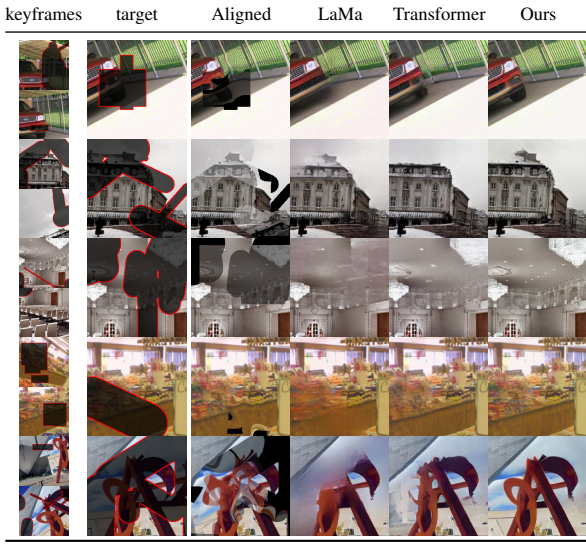
| keyframes | target | Aligned | LaMa | Transformer | Ours |

Figure 3. Qualitative results on guided image inpainting.

3. Approach

Our goal is to develop a model that can propagate information from keyframes to target frames. Let $x_{\text{tgt}} \in \mathbb{R}^{H_{\text{in}} \times W_{\text{in}} \times C_{\text{tgt}}}$ be the target frame and $x_{\text{src}} \in \mathbb{R}^{T \times H_{\text{in}} \times W_{\text{in}} \times C_{\text{src}}}$ be a sequence of keyframes. For inpainting, $C_{\text{tgt}} = C_{\text{src}} = 4$, containing RGB intensities of masked frames and the mask. The completion of the target frame depends on unmasked content from both x_{tgt} and x_{src}.

3.1. Feature Encoding and Decoding

LIF Encoding The main goal of the LIF stream is to preserve and propagate high-frequency details. To initialize this stream, we follow previous works and use a strided convolutional architecture to extract features from the inputs. By keeping the stride s relatively small while expanding the number of feature channels c, (in practice we use a stride $s = 8$ with $c = 512$ channels), these features, together with a similar deconvolutional architecture, provide an almost lossless feature encoding. We encode each keyframe and the target frame individually and model interactions only afterwards. Thus, every frame represented in the LIF stream by $h_{\text{LIF}}^0 \in \mathbb{R}^{H \times W \times c}$, where $H = \frac{H_{\text{in}}}{s}$ and $W = \frac{W_{\text{in}}}{s}$.

GIF Initialization The goal of the GIF stream is to model robust low-frequency interactions within and across frames. We initialize this stream with a set of learned parameters $h_{\text{GIF}}^0 \in \mathbb{R}^{M \times d}$, where M is the sequence length and controls the computational complexity of the stream. The learned parameters serve as a positional encoding.

Decoding The encoding stage results in two feature representations, $h_{\text{LIF}}^0, h_{\text{GIF}}^0 = f_{\text{enc}}(x)$ for each frame x. These will be processed by a sequence of L blocks which produce $h_{\text{LIF}}^L, h_{\text{GIF}}^L$. The final output is then predicted from the h_{LIF}^L representation of the target frame, i.e. $y = f_{\text{dec}}(h_{\text{LIF}}^L)$. Next, we describe how the blocks map $h_{\text{LIF}}^i, h_{\text{GIF}}^i \mapsto h_{\text{LIF}}^{i+1}, h_{\text{GIF}}^{i+1}$.

3.2. Intra-Frame and Inter-Stream Interactions

The LIF stream consists of convolutional residual blocks for local interaction, while the GIF stream consists of attention blocks for global interactions. Read and write operations exchange complementary features between them.

Read Operation Since generally $M < N := H \cdot W$, we have to average LIF features or select a subset of them to read into the GIF stream. We use a read module that learns how to read features from the LIF into the GIF stream.

We assume that $M = m^2$ is a square number and that $H \equiv 0 \mod m$ and $W \equiv 0 \mod m$ (otherwise interpolating to the closest height and width that is divisible by m). We divide the LIF feature map into M equal-sized patches and learn which features of the j-th patch to read into the j-th GIF feature by forming an importance weighted sum of projected features. If $P_j \in \mathbb{R}^{(\frac{H}{m} \cdot \frac{W}{m}) \times c}$ is the j-th patch,

$$\text{read}(P_j) = \text{softmax}(W_S P_j^t) P_j W_V, \qquad (1)$$

where $W_S \in \mathbb{R}^{1 \times c}$ and $W_V \in \mathbb{R}^{c \times d}$ are learnable weights. We follow common design choices of attention and (i) use multiple read heads with their own score and value projections and (ii) apply a Layer Normalization followed by a linear projection and a residual connection on the GIF stream.

Write Operation After processing the GIF stream with attention blocks, we write the result back into the high-capacity LIF stream. We use a similar approach as for the read operation, except that the attention weights are now computed on the transposed patch and values are computed from the GIF stream. If $P_j \in \mathbb{R}^{(\frac{H}{m} \cdot \frac{W}{m}) \times c}$ is the j-th LIF patch and $G_j \in \mathbb{R}^{1 \times d}$ is the j-th GIF feature,

$$\text{write}(P_j, G_j) = \text{sigmoid}(P_j W_S^t) G_j W_V^t, \qquad (2)$$

with $W_S \in \mathbb{R}^{1 \times c}$ and $W_V \in \mathbb{R}^{c \times d}$. As in the read operation, we use multiple write heads followed by layer norm, projection, and a residual connection on the LIF stream.

Together, a read operation, local and global interactions in the LIF and GIF streams, followed by a write operation represent one intra-frame block as shown in Fig. 2.

3.3. Cross-Frame Interactions

Global Cross-Frame Propagation To propagate information from keyframes to the target, we replace self-attention in the GIF stream with cross-attention. We use a symmetric design, where the same block is used for self-attention on keyframes and for cross-attention on target frames, by concatenating keys and values from keyframes. If $g_{\text{src}} \in \mathbb{R}^{M \times d}$ and $g_{\text{tgt}} \in \mathbb{R}^{M \times d}$ denote GIF features from a keyframe and the target frame, respectively, we compute the attention operation A for keyframes and target as

$$A(g_{\text{src}}, \varnothing) = \text{softmax}(g_{\text{src}} W_Q^t (g_{\text{src}} W_K^t)^t)(g_{\text{src}} W_V)$$

$$A(g_{\text{tgt}}, g_{\text{src}}) = \text{softmax}(g_{\text{tgt}} W_Q^t ([g_{\text{tgt}}, g_{\text{src}}] W_K^t)^t)[g_{\text{tgt}}, g_{\text{src}}] W_V,$$

with $W_Q \in \mathbb{R}^{d_k \times d}$, $W_K \in \mathbb{R}^{d_k \times d}$, and $W_V \in \mathbb{R}^{d \times d}$.

Method	FID ↓	LPIPS ↓	SSIM ↑
Transformer	15.19	0.173± 0.072	0.814± 0.097
Ours w/o FFC	14.19	0.155± 0.075	0.831± 0.096
LaMa	<u>13.73</u>	<u>0.147</u>± 0.077	<u>0.836</u>± 0.096
Ours	**13.15**	**0.145**± 0.074	**0.837**± 0.095

Table 1. Single Image Inpainting Results on Places [40].

Method	FID ↓	LPIPS ↓	SSIM ↑
LaMa + SpectralFuse	26.40	0.211± 0.115	0.794± 0.138
Transformer	18.18	0.175± 0.094	0.821± 0.128
Our w/o FFC	<u>14.78</u>	<u>0.140</u>± 0.082	**0.851**± 0.110
Ours	**14.29**	**0.137**± 0.080	<u>0.848</u>± 0.110
Ours (big)	13.09	0.130± 0.074	0.865± 0.101

Table 2. Guided Image Inpainting Results on Places [40].

Method	FID ↓	LPIPS ↓	SSIM ↑	VFID ↓	PVCS ↓	PCons ↑
Ours $_{14+prealign}$	**4.34**	**0.0034**	**0.9630**	0.0543	<u>0.2263</u>	42.39
Ours $_{14}$	<u>4.45</u>	<u>0.0042</u>	<u>0.9597</u>	<u>0.0542</u>	0.2339	41.45
Ours $_6$	4.68	0.0051	0.9581	0.0561	0.2443	41.14
LaMa [27] $_{+flow}$	5.28	0.0082	0.9459	0.0877	0.3151	40.22
DFCNet [33]	7.71	0.0054 (0.0056)	0.9500	0.0627	**0.2240**	**57.80**
E2FGVI [16]	8.22	0.0046	0.9585	0.0613	0.2519	33.19
FGVC [8]	9.76	0.0065 (0.0054)	0.9548	0.0564	0.2322	38.26
JointOpt [9]	7.30	0.0058 (0.0059)	0.9559	**0.0530**	0.2324	37.19
OPN [23]	8.71	0.0062 (0.0057)	0.9525	0.0708	0.2874	35.09
CPNet [14]	13.21	0.0056 (0.0068)	0.9574	0.0969	0.3048	43.91
STTN [35]	10.89	0.0083 (0.0065)	0.9542	0.0911	0.3149	41.12
VINet [13]	23.63	0.0090 (0.0084)	0.9481	0.1488	0.4312	<u>50.07</u>

Table 3. Video Inpainting Result on DEVIL [28].

Deformable Write Operation To overcome limitations of attention-based propagation of high-frequency features, we introduce a complementary approach based on an explicit alignment with a deformable write module that fuses LIF features from keyframes into those of the target frame.

Let $h_{\text{LIF}}^i \in \mathbb{R}^{H \times W \times c}$ denote LIF features of keyframe i, and $\phi_i \in \mathbb{R}^{H \times W \times 2}$ a flow field such that a position p in the target frame corresponds to the position $p + \phi_i(p)$ in the i-th keyframe. We write $[h_{\text{LIF}}^i(p + \phi_i(p))] \in \mathbb{R}^{T \times c}$ to denote the stacked, bilinearly interpolated values of h_{LIF}^i at positions $p + \phi_i(p)$. The deformable write operation then aggregates these interpolated features based on confidence scores,

$$\sum \text{softmax}([h_{\text{LIF}}^i(p + \phi_i(p))]W_Q^T) \odot [h_{\text{LIF}}^i(p + \phi_i(p))]W_V$$

where $\odot$ is elementwise multiplication, $W_Q \in \mathbb{R}^{c \times c}$ and $W_V \in \mathbb{R}^{c \times c}$ are learnable parameters, and the sum and softmax are applied along the stacked dimension. The result is added to the LIF feature stream of the target frame.

In contrast to global cross-frame interaction, this operation can propagate high-frequency details but it is also more susceptible to errors due to wrongly estimated flow fields ϕ_i. For the estimation of confidence scores, we thus concatenate forward-backward consistency values of the flow field. The flow fields are estimated with a pre-trained optical flow model [29] operating at a fixed resolution of 256×256 and interpolated to the spatial size of the LIF features.

4. Experiments

We evaluate the propagation capabilities of our model on different inpainting tasks. Image inpainting requires context propagation within a frame, while guided inpainting and video inpainting require context propagation across frames to predict plausible and consistent content in masked areas.

We use LaMa [27], which relies on Fast Fourier Convolutions (FFCs) to take global context into account, as a strong baseline and follow its training and evaluation protocol based on the Places dataset [40]. Tab. 1 compares the inpainting performance of different approaches under the same computational budget, which is calibrated through the number of blocks. A transformer approach, which is similar to our model without the LIF stream, performs worst, demonstrating its difficulties to faithfully propagate context. Our approach with spatial convolutions in the LIF stream (Ours w/o FFC) improves performance but achieves worse performance than LaMa. However, in combination with FFCs in the LIF stream (Ours), our model achieves the best performance, suggesting complementary properties of spectral convolutions and propagation capabilities.

To evaluate context propagation across frames, we generate two synthetic keyframes for each example by applying random transformations, deformations, and masks. We further investigate propagation in the spectral domain and include a variant of LaMa that aggregates Fourier features across frames (Lama+SpectralFuse). Both the quantitative results in Tab. 2, as well as the qualitative results in Fig. 3 show that this fails to propagate context unless a keyframe happens to be aligned with the target frame (second row in Fig. 3). The transformer-based approach can take keyframe-context into account but fails to propagate high-frequency details. Our approach performs significantly better than these two baselines both with and without FFCs, which demonstrates the improved propagation capabilities.

Finally, we evaluate how well our approach generalizes to real videos. We train a bigger variant of our best performing model for guided inpainting (Ours (big)), and use it to generate every 20th frame of a masked video. The remaining frames are propagated based on optical flow. We use the DEVIL evaluation [28] to compare different approaches in Tab. 3. The subscript indicates the number of keyframes used. We also include results obtained by propagating frames inpainted without context as *Lama [27]+flow*. Overall, we observe increasing performance with an increasing number of keyframes available, which demonstrates that our approach is able to propagate context across frames and that this leads to improved video inpainting performance.

5. Conclusion

We propose a novel approach for keyframe propagation based on a two-stream approach, where one stream models the local interactions of high-frequency features and the other models the global interactions of low-frequency features. We show that this method improves image and video inpainting performance. We are investigating applications of this architecture to other tasks such as object segmentation and matting, with the goal to find a unified approach.

References

[1] Aseem Agarwala, Aaron Hertzmann, D. Salesin, and Steven M. Seitz. Keyframe-based tracking for rotoscoping and animation. In *SIGGRAPH 2004*, 2004. 2

[2] Connelly Barnes, Eli Shechtman, Adam Finkelstein, and Dan B. Goldman. Patchmatch: a randomized correspondence algorithm for structural image editing. In *SIGGRAPH 2009*, 2009. 2

[3] Sergi Caelles, Kevis-Kokitsi Maninis, Jordi Pont-Tuset, Laura Leal-Taixé, Daniel Cremers, and Luc Van Gool. One-shot video object segmentation. *2017 IEEE Conference on Computer Vision and Pattern Recognition (CVPR)*, pages 5320–5329, 2017. 2

[4] Ho Kei Cheng, Yu-Wing Tai, and Chi-Keung Tang. Rethinking space-time networks with improved memory coverage for efficient video object segmentation. In *NeurIPS*, 2021. 1

[5] Krzysztof Choromanski, Valerii Likhosherstov, David Dohan, Xingyou Song, Andreea Gane, Tamás Sarlós, Peter Hawkins, Jared Davis, Afroz Mohiuddin, Lukasz Kaiser, David Belanger, Lucy J. Colwell, and Adrian Weller. Rethinking attention with performers. *CoRR*, abs/2009.14794, 2020. 2

[6] Alexey Dosovitskiy, Lucas Beyer, Alexander Kolesnikov, Dirk Weissenborn, Xiaohua Zhai, Thomas Unterthiner, Mostafa Dehghani, Matthias Minderer, Georg Heigold, Sylvain Gelly, et al. An image is worth 16x16 words: Transformers for image recognition at scale. *arXiv preprint arXiv:2010.11929*, 2020. 2

[7] Patrick Esser, Robin Rombach, and Bjorn Ommer. Taming transformers for high-resolution image synthesis. In *Proceedings of the IEEE/CVF Conference on Computer Vision and Pattern Recognition (CVPR)*, pages 12873–12883, June 2021. 2

[8] Chen Gao, Ayush Saraf, Jia-Bin Huang, and Johannes Kopf. Flow-edge guided video completion. In *ECCV*, 2020. 2, 4, 7, 11, 12, 13

[9] Jia-Bin Huang, Sing Bing Kang, Narendra Ahuja, and Johannes Kopf. Temporally coherent completion of dynamic video. *ACM Transactions on Graphics (TOG)*, 35:1 – 11, 2016. 2, 4, 7

[10] Andrew Jaegle, Felix Gimeno, Andy Brock, Oriol Vinyals, Andrew Zisserman, and Joao Carreira. Perceiver: General perception with iterative attention. In *International Conference on Machine Learning*, pages 4651–4664. PMLR, 2021. 1, 2

[11] Andrej Karpathy. The ongoing consolidation in AI is incredible. https://twitter.com/karpathy/status/1468370605229547522. Accessed: 2022-03-19. 1

[12] Salman H. Khan, Muzammal Naseer, Munawar Hayat, Syed Waqas Zamir, Fahad Shahbaz Khan, and Mubarak Shah. Transformers in vision: A survey. *CoRR*, abs/2101.01169, 2021. 2

[13] Dahun Kim, Sanghyun Woo, Joon-Young Lee, and In So Kweon. Deep video inpainting. *2019 IEEE/CVF Conference on Computer Vision and Pattern Recognition (CVPR)*, pages 5785–5794, 2019. 2, 4, 7

[14] SungHo Lee, Seoung Wug Oh, DaeYeun Won, and Seon Joo Kim. Copy-and-paste networks for deep video inpainting. *2019 IEEE/CVF International Conference on Computer Vision (ICCV)*, pages 4412–4420, 2019. 2, 4, 7

[15] Anat Levin, Dani Lischinski, and Yair Weiss. Colorization using optimization. *ACM SIGGRAPH 2004 Papers*, 2004. 2

[16] Zhen Li, Cheng-Ze Lu, Jianhua Qin, Chun-Le Guo, and Ming-Ming Cheng. Towards an end-to-end framework for flow-guided video inpainting. In *IEEE Conference on Computer Vision and Pattern Recognition (CVPR)*, 2022. 4, 7, 11, 12, 13

[17] Ze Liu, Yutong Lin, Yue Cao, Han Hu, Yixuan Wei, Zheng Zhang, Stephen Lin, and Baining Guo. Swin transformer: Hierarchical vision transformer using shifted windows. In *Proceedings of the IEEE/CVF International Conference on Computer Vision*, pages 10012–10022, 2021. 2

[18] Yuqing Ma, Xianglong Liu, Shihao Bai, Le-Yi Wang, Aishan Liu, Dacheng Tao, and Edwin Hancock. Region-wise generative adversarial imageinpainting for large missing areas. *ArXiv*, abs/1909.12507, 2019. 2

[19] Simone Meyer, Victor Cornillère, Abdelaziz Djelouah, Christopher Schroers, and Markus H. Gross. Deep video color propagation. In *BMVC*, 2018. 2

[20] Charlie Nash, Jacob Menick, Sander Dieleman, and Peter W. Battaglia. Generating images with sparse representations. *CoRR*, abs/2103.03841, 2021. 2

[21] Kamyar Nazeri, Eric Ng, Tony Joseph, Faisal Z. Qureshi, and Mehran Ebrahimi. Edgeconnect: Generative image inpainting with adversarial edge learning. *ArXiv*, abs/1901.00212, 2019. 2

[22] Seoung Wug Oh, Joon-Young Lee, N. Xu, and Seon Joo Kim. Video object segmentation using space-time memory networks. *2019 IEEE/CVF International Conference on Computer Vision (ICCV)*, pages 9225–9234, 2019. 1, 2

[23] Seoung Wug Oh, SungHo Lee, Joon-Young Lee, and Seon Joo Kim. Onion-peel networks for deep video completion. *2019 IEEE/CVF International Conference on Computer Vision (ICCV)*, pages 4402–4411, 2019. 2, 4, 7

[24] Namuk Park and Songkuk Kim. How do vision transformers work? In *International Conference on Learning Representations*, 2022. 2

[25] F. Perazzi, J. Pont-Tuset, B. McWilliams, L. Van Gool, M. Gross, and A. Sorkine-Hornung. A benchmark dataset and evaluation methodology for video object segmentation. In *Computer Vision and Pattern Recognition*, 2016. 7, 11, 12, 13

[26] Alec Radford, Karthik Narasimhan, Tim Salimans, and Ilya Sutskever. Improving language understanding by generative pre-training. 2018. 2

[27] Roman Suvorov, Elizaveta Logacheva, Anton Mashikhin, Anastasia Remizova, Arsenii Ashukha, Aleksei Silvestrov, Naejin Kong, Harshith Goka, Kiwoong Park, and Victor S. Lempitsky. Resolution-robust large mask inpainting with fourier convolutions. *ArXiv*, abs/2109.07161, 2021. 1, 2, 4, 7, 11, 12, 13

[28] Ryan Szeto and Jason J. Corso. The DEVIL is in the details: A diagnostic evaluation benchmark for video inpainting. *CoRR*, abs/2105.05332, 2021. 4, 7

[29] Zachary Teed and Jia Deng. RAFT: recurrent all-pairs field transforms for optical flow. *CoRR*, abs/2003.12039, 2020. 4

[30] Ashish Vaswani, Noam Shazeer, Niki Parmar, Jakob Uszkoreit, Llion Jones, Aidan N. Gomez, Lukasz Kaiser, and Illia Polosukhin. Attention is all you need. 2017. 1, 2

[31] Sinong Wang, Belinda Z Li, Madian Khabsa, Han Fang, and Hao Ma. Linformer: Self-attention with linear complexity. *arXiv preprint arXiv:2006.04768*, 2020. 2

[32] Yonatan Wexler, Eli Shechtman, and Michal Irani. Space-time completion of video. *IEEE Transactions on Pattern Analysis and Machine Intelligence*, 29, 2007. 2

[33] Rui Xu, Xiaoxiao Li, Bolei Zhou, and Chen Change Loy. Deep flow-guided video inpainting. *2019 IEEE/CVF Conference on Computer Vision and Pattern Recognition (CVPR)*, pages 3718–3727, 2019. 2, 4, 7, 11, 12, 13

[34] Jiahui Yu, Zhe L. Lin, Jimei Yang, Xiaohui Shen, Xin Lu, and Thomas S. Huang. Free-form image inpainting with gated convolution. *2019 IEEE/CVF International Conference on Computer Vision (ICCV)*, pages 4470–4479, 2019. 2

[35] Yanhong Zeng, Jianlong Fu, and Hongyang Chao. Learning joint spatial-temporal transformations for video inpainting. *ArXiv*, abs/2007.10247, 2020. 2, 4, 7

[36] Yanhong Zeng, Jianlong Fu, Hongyang Chao, and Baining Guo. Aggregated contextual transformations for high-resolution image inpainting. *ArXiv*, abs/2104.01431, 2021. 2

[37] Richard Zhang, Jun-Yan Zhu, Phillip Isola, Xinyang Geng, Angela S. Lin, Tianhe Yu, and Alexei A. Efros. Real-time user-guided image colorization with learned deep priors. *ACM Transactions on Graphics (TOG)*, 36:1 – 11, 2017. 2

[38] Shengyu Zhao, Jianwei Cui, Yilun Sheng, Yue Dong, Xiao Liang, Eric I-Chao Chang, and Yan Xu. Large scale image completion via co-modulated generative adversarial networks. *ArXiv*, abs/2103.10428, 2021. 2

[39] Yunhan Zhao, Connelly Barnes, Yuqian Zhou, Eli Shechtman, Sohrab Amirghodsi, and Charless Fowlkes. Geofill: Reference-based image inpainting of scenes with complex geometry. *arXiv preprint arXiv:2201.08131*, 2022. 2

[40] Bolei Zhou, Àgata Lapedriza, Aditya Khosla, Aude Oliva, and Antonio Torralba. Places: A 10 million image database for scene recognition. *IEEE Transactions on Pattern Analysis and Machine Intelligence*, 40:1452–1464, 2018. 4, 7

[41] Yuqian Zhou, Connelly Barnes, Eli Shechtman, and Sohrab Amirghodsi. Transfill: Reference-guided image inpainting by merging multiple color and spatial transformations. In *Proceedings of the IEEE/CVF Conference on Computer Vision and Pattern Recognition (CVPR)*, pages 2266–2276, June 2021. 2

Supplementary Materials

We include additional details on the evaluations in Sec. A and additional qualitative results in Sec. B. Implementation details and video results can be found at https://github.com/runwayml/guided-inpainting.

A. Evaluation Details

(Guided) Image Inpainting In Tab. 1 and 2, we use a subset of 2k images from the Places [40] validation split at a resolution of 256×256 pixels. *Ours (big)* uses two cross-frame blocks and 12 intra-frame blocks, all other models use two cross-frame blocks and four intra-frame blocks. We train models with a learning rate of $3.2 \cdot 10^{-4}$ and an effective batch size of 32, accumulated over two batches and distributed across two V100 GPUs.

For guided inpainting, we use two keyframes during training and four for the evaluation in Tab. 2. Evaluation results with two keyframes can be found in Tab. 4. The performance of all methods improves as context from more keyframes becomes available and their relative performance-ordering to one another remains the same.

Video Inpainting For the evaluation in Tab. 3, we use the evaluation code[1] provided by the DEVIL benchmark [28]. We use the 'flickr-all' video subset combined with the 'fvi-fgs-h' mask subset which contains large inpainting masks and represents a challenging setting. For DFCNet [33], FGVC [8], JointOpt [9], OPN [23], CPNet [14], STTN [35] and VINet [13] we use the pre-computed inpainting results on 'flickr-all_fvi-fgs-h' provided by [28] and recompute the metrics. This reproduces the results reported in [28] except for the LPIPS metrics, for which we include the results from [28] in parentheses.

In addition, we compute inpainting results from concurrent video inpainting work E2FGVI [16] using their provided code[2] and *E2FGVI-HQ* checkpoint.

The *Ours* entries in Tab. 3 always refer to results computed with the *Ours (big)* checkpoint that contains 12 intra-frame blocks. The number in the subscript indicates the number of keyframes. For 6, we use frames with offsets $\pm\{10, 20, 40\}$, and for 14, we use frames with offsets $\pm\{5, 10, 15, 20, 40, 60, 80\}$ to capture more context from the video. The subscript +prealign refers to an extra step of manually fusing context from other frames in areas where the optical flow is reliable. This brings some additional gains and hints that there is still room for improvement regarding the propagation of high-frequency details from other frames. We hypothesize that deformable writes on higher-resolution feature maps and/or the use of skip connections in the architecture could further improve the propagation capabilities.

To evaluate the importance of taking context from keyframes into account for video inpainting, we also include *LaMa [27]+flow*, which uses the *big-lama* checkpoint, provided[3] by the authors of [27], in combination with the same flow-propagation of intermediate frames as for the *Ours* entries. This represents a strong non-guided baseline for video inpainting which can achieve relatively good FID scores but fails to take the context from the video into account as indicated by bad LPIPS scores. With the ability to take context from other frames into account, our approach can achieve the best scores for both measures.

Method	FID $\downarrow$	LPIPS $\downarrow$	SSIM $\uparrow$
LaMa + SpectralFuse	26.74	0.212 ± 0.116	0.759 ± 0.139
Transformer	18.87	0.181 ± 0.096	0.802 ± 0.130
Our w/o FFC	<u>17.62</u>	<u>0.157</u> ± 0.091	**0.833** ± 0.118
Ours	**16.90**	**0.154** ± 0.089	<u>0.834</u> ± 0.118
Ours (big)	15.45	0.148 ± 0.084	0.849 ± 0.111

Table 4. Guided Image Inpainting Results on Places [40] using two keyframes.

B. Qualitative Results

We include additional qualitative results for guided image inpainting in Fig. 5 and 4, and a larger version of Fig. 3 in Fig. 6. For video inpainting, we show qualitative results for DAVIS [25] sequences in Fig. 7-9. Animated versions for all DAVIS sequences can be found online at https://github.com/runwayml/guided-inpainting. The results of other methods for these sequences are taken from the online supplementary[4] of [8] when available and recomputed otherwise.

---

[1] https://github.com/MichiganCOG/devil
[2] https://github.com/MCG-NKU/E2FGVI
[3] https://github.com/saic-mdal/lama
[4] https://filebox.ece.vt.edu/~chengao/FGVC/pages/object_removal.html

Note that the long-term temporal stability of our method is reduced compared to other approaches, because we compute each chunk of 20 frames from the video independently. This gives computational speed advantages by enabling parallelization over chunks as opposed to a fully sequential processing required by other approaches. On shorter timescales, the animated versions demonstrate that our approach exhibits significantly less short-term temporal instabilities like flickering.
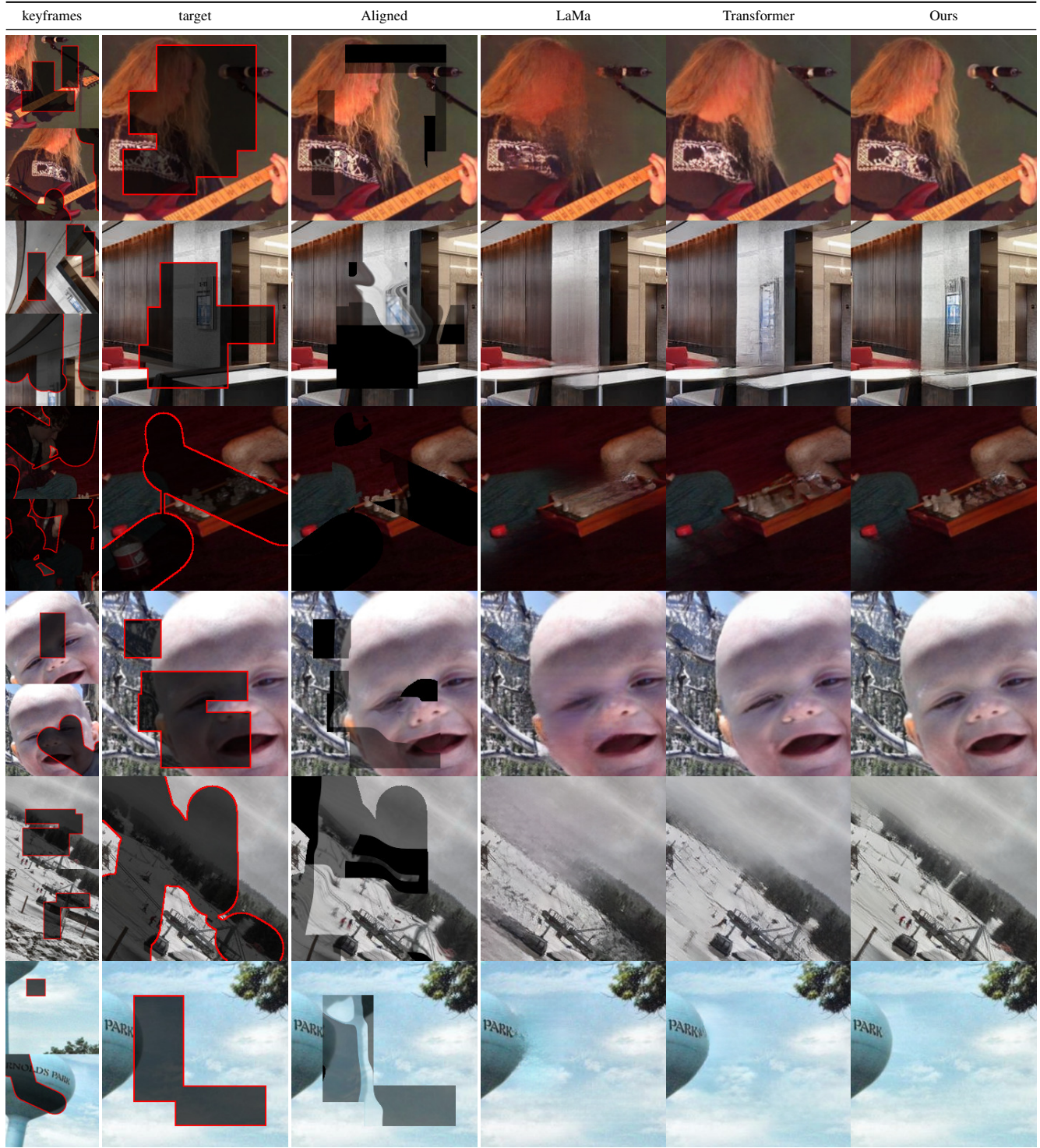

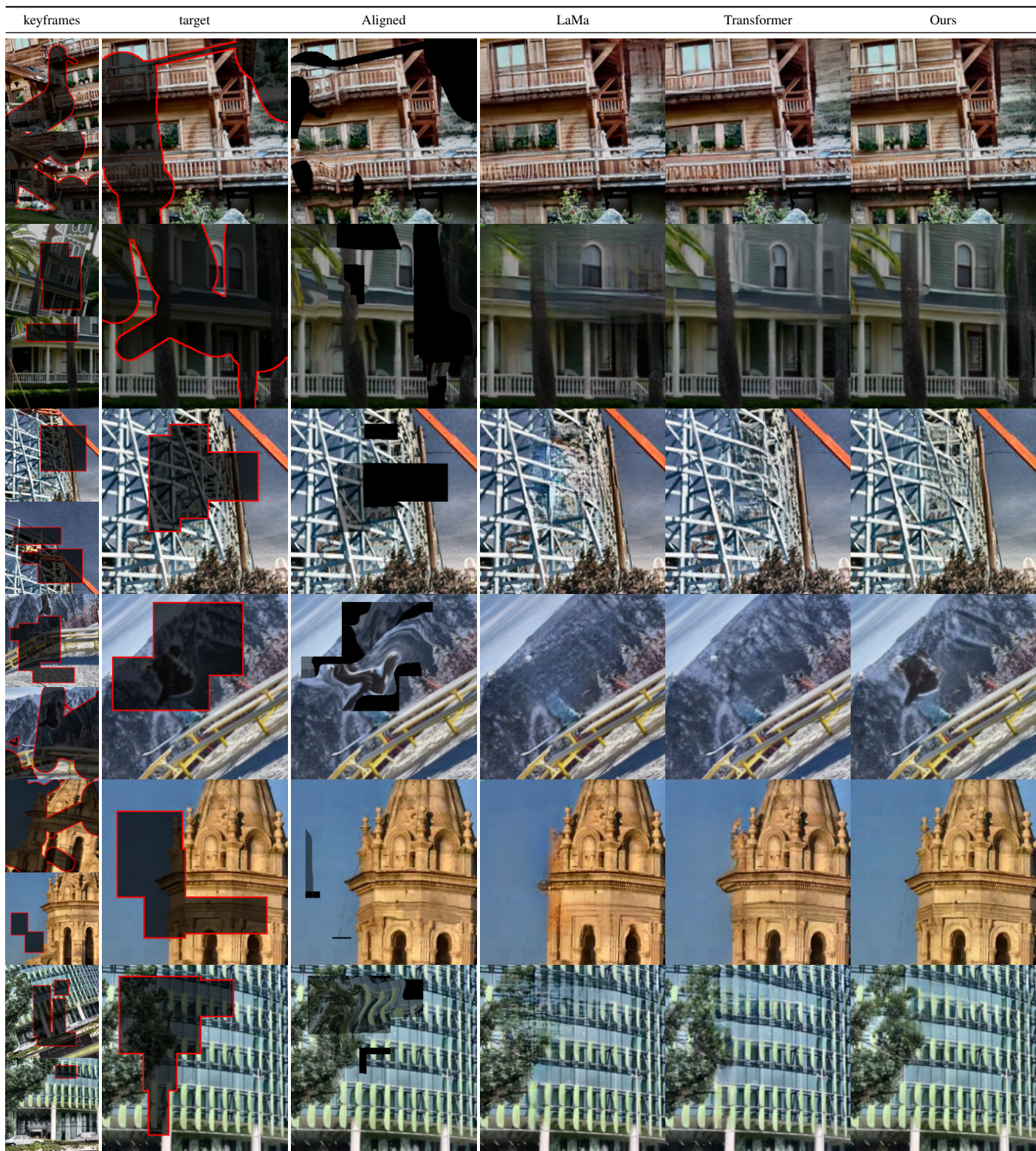Figure 4. Qualitative results on guided image inpainting.

keyframes	target	Aligned	LaMa	Transformer	Ours

Figure 5. Qualitative results on guided image inpainting.

keyframes	target	Aligned	LaMa	Transformer	Ours
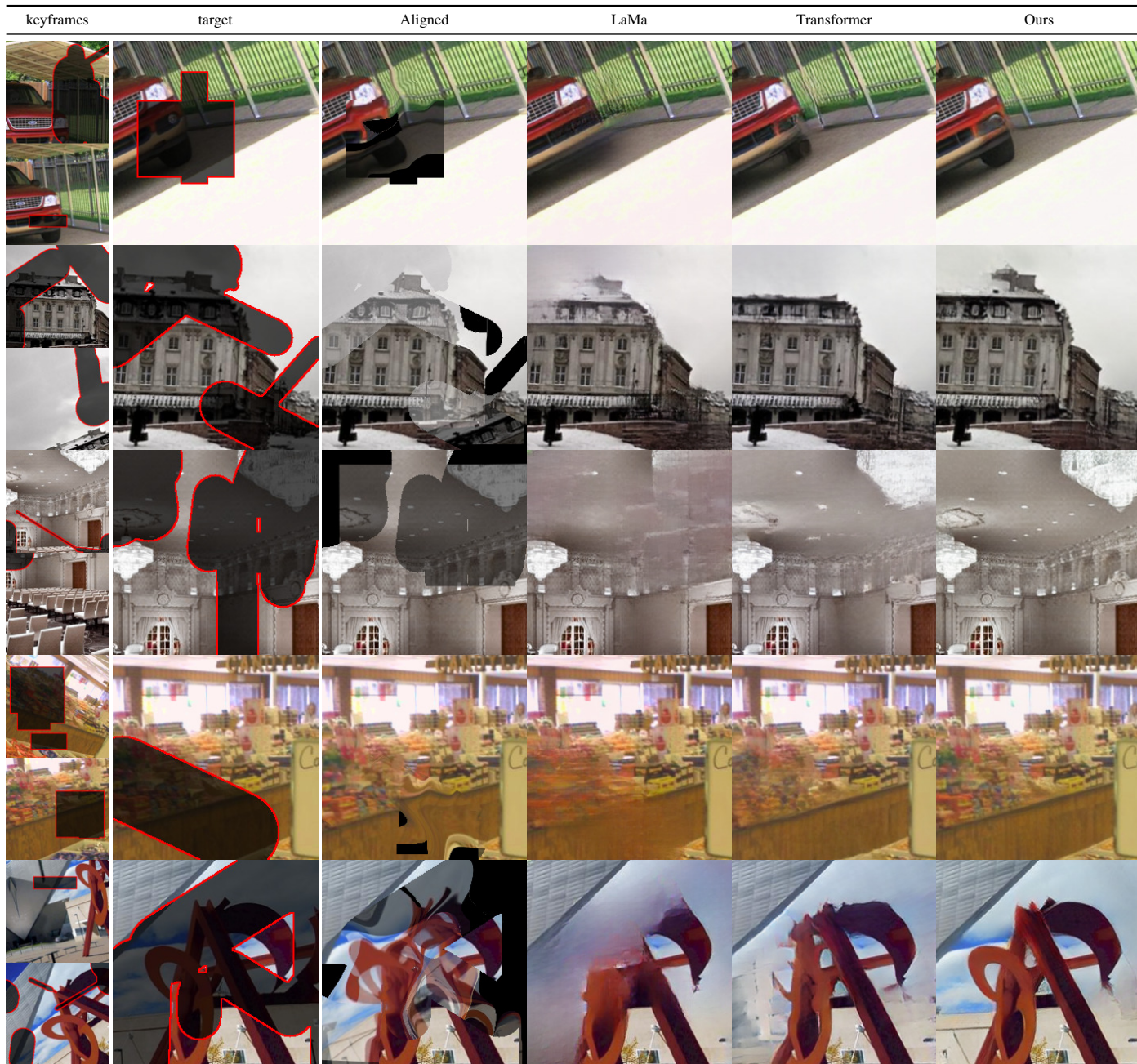
Figure 6. A larger version of Fig. 3.

	Frames
input	
Ours 14+prealign	
Ours 14	
LaMa [27] +flow	
DFCNet [33]	
E2FGVI [16]	
FGVC [8]	
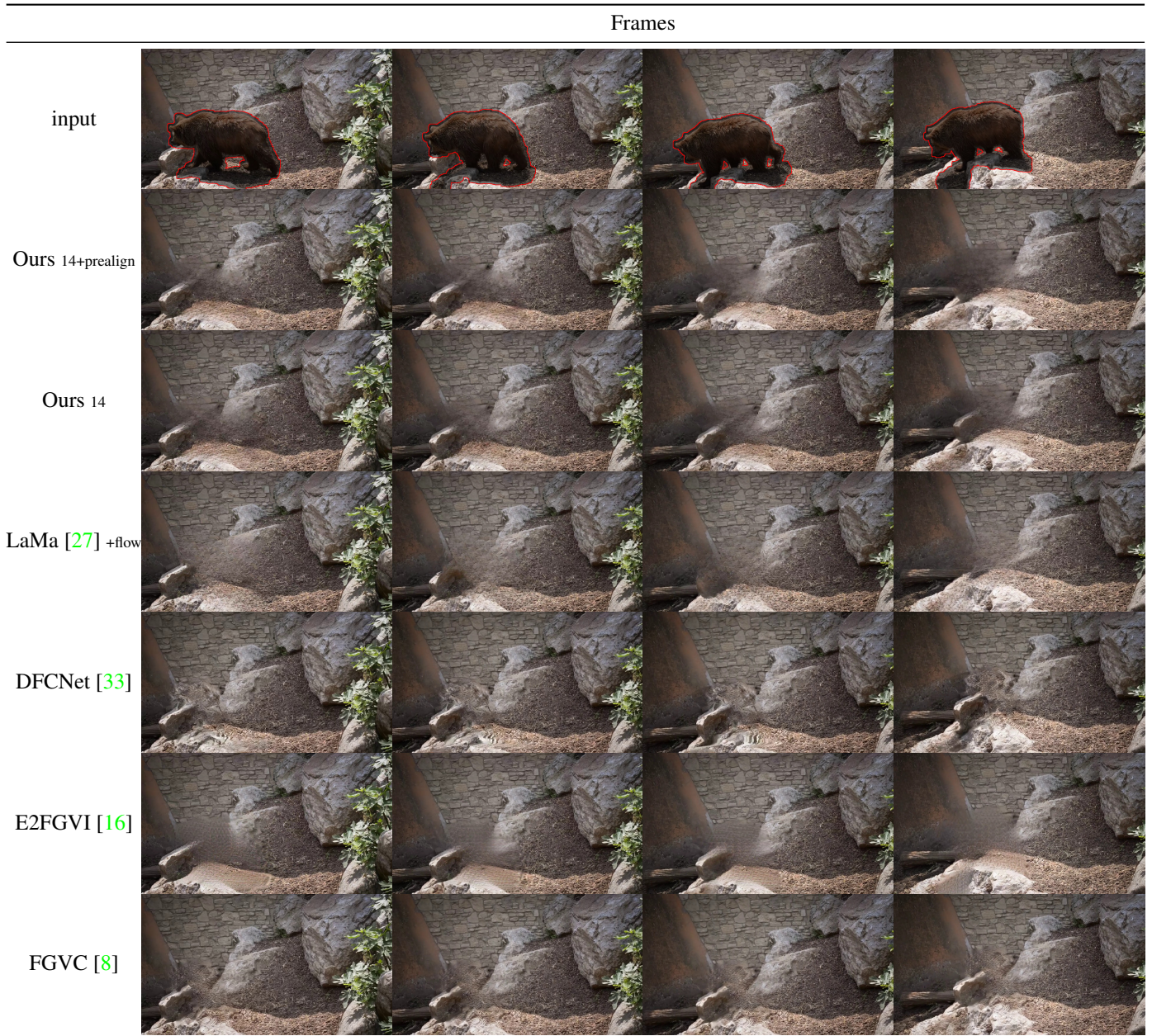
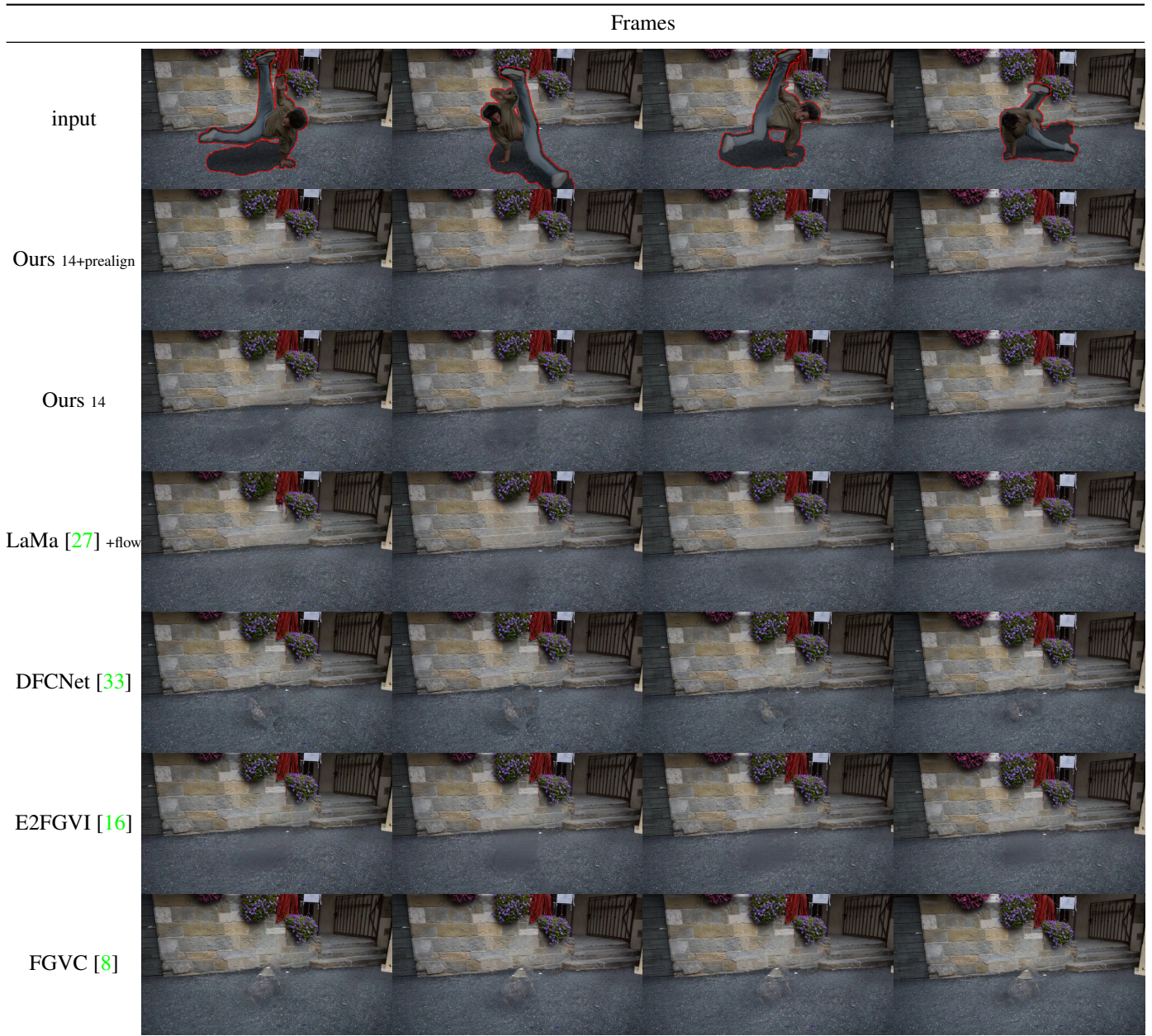Figure 7. Qualitative results for video inpainting on the DAVIS [25] sequence *bear*. Animated version at https://github.com/runwayml/guided-inpainting.

Figure 8. Qualitative results for video inpainting on the DAVIS [25] sequence *breakdance-flare*. Animated version at https://github.com/runwayml/guided-inpainting.
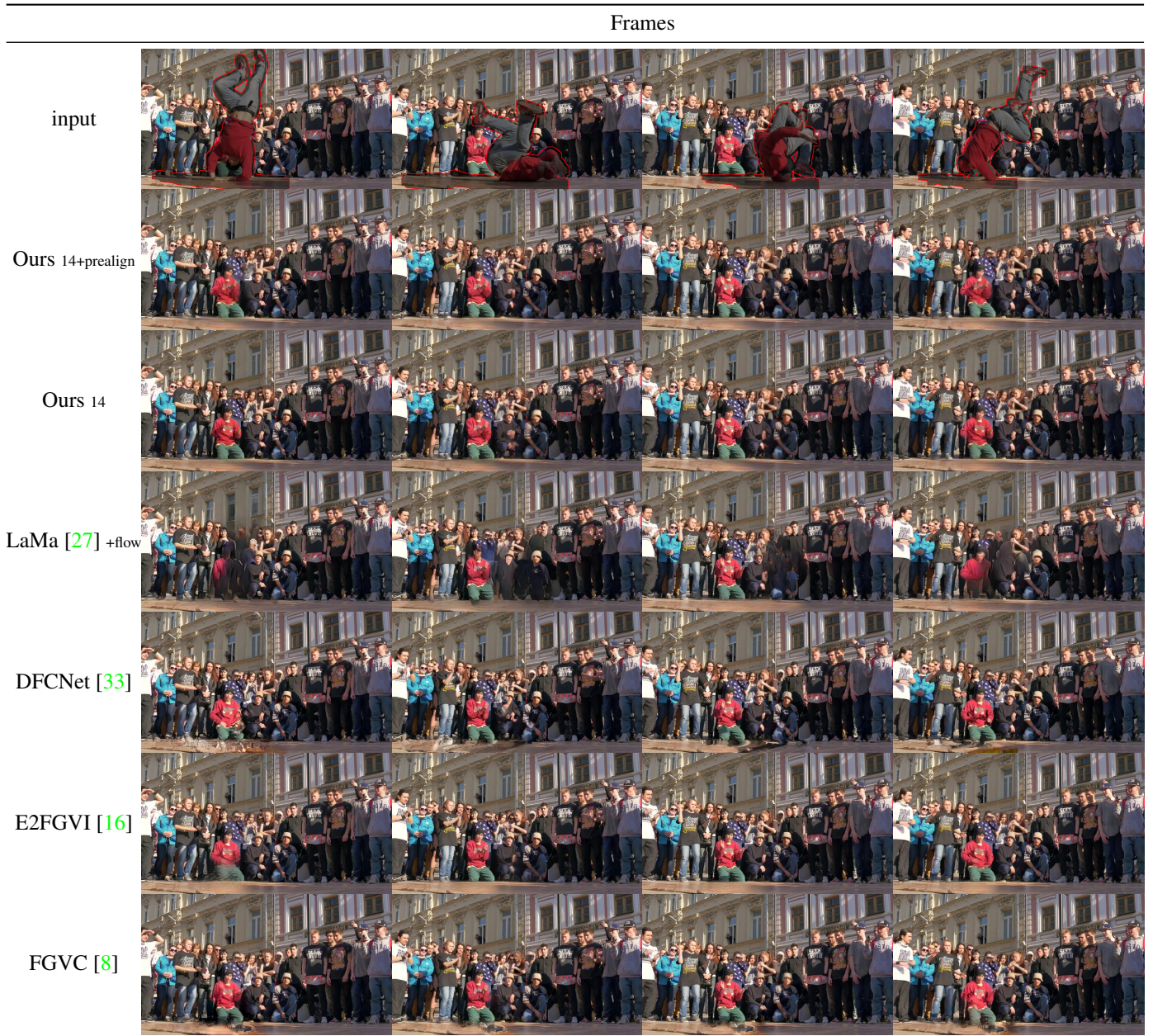
Figure 9. Qualitative results for video inpainting on the DAVIS [25] sequence *breakdance*. Animated version at https://github.com/runwayml/guided-inpainting.